JOURNAL OF AIRCRAFT
Vol. 38, No. 3, May–June 2001

Compressible Dynamic Stall Control: Comparison of Two Approaches

M. S. Chandrasekhara*
Navy–NASA Joint Institute of Aeronautics, Naval Postgraduate School, Monterey, California 93943
M. C. Wilder†
ELORET, Sunnyvale, California 94087
and
L. W. Carr‡
U.S. Army Aeroflightdynamics Directorate, NASA Ames Research Center, Moffett Field, California 94035

The approaches of compressible dynamic stall control using real-time airfoil adaptation and slatted airfoils are compared. Each method attempts to solve the unsteady flow separation and the underlying causes differently. The approaches lead to unexpected results: For the slatted airfoil, dynamic stall alleviation on the main airfoil with a fully stalled slat occurred, and for the shape adapting airfoil, leading-edge attached flow with trailing-edge separation was obtained. In both cases, no dynamic stall vortex was present. As can be expected, the control effectiveness of each method varies over the full cycle and depends on the Mach number due to the new factors introduced by the use of the methods. These issues are addressed.

Nomenclature

C_p	=	pressure coefficient
$C_{p_{\min}}$	=	peak suction pressure coefficient
c	=	airfoil chord
f	=	frequency of oscillation, Hz
k	=	reduced frequency, $\pi f c/U_\infty$
M	=	freestream Mach number
p	=	static pressure
Re	=	Reynolds number based on chord
s, n	=	coordinates along and normal to airfoil surface
t	=	time
U_S	=	tangential surface velocity
U_∞	=	freestream velocity
V	=	suction or blowing velocity
x, y	=	chordwise and vertical distance
α	=	angle of attack
ν	=	kinematic viscosity
ρ	=	density
Ω	=	spanwise component of vorticity
ω	=	circular frequency

I. Introduction

THE problem of compressible dynamic stall control is of considerable interest to both helicopter and fighter aircraft aerodynamicists.[1] Incompressible dynamic stall also has direct application in renewable energy systems such as wind turbines.[1] Research completed thus far[2] has clearly established that the onset of dynamic stall is very sensitive to flow conditions such as freestream Mach number, reduced frequency, Reynolds number, and leading-edge curvature.[3,4] When compressibility effects arise ($M > 0.2$), the stall onset mechanism changes dramatically depending on the flow conditions. At low Reynolds numbers and Mach numbers, it arises from a large leading-edge adverse pressure gradient. At slightly higher values of these quantities, when the local flow becomes supersonic, the mechanism changes to that due to an interaction between the local supersonic flow and the laminar separation bubble, at very low pressure gradients. Tripping the airfoil causes dynamic stall again from the strong leading-edge adverse pressure gradient. At higher Mach numbers, shock-induced separation initiates dynamic stall.

A rotor blade encounters a variety of freestream conditions depending on the local flow conditions. Hence, it may see dynamic stall arising from any of these causes. In general, at higher Reynolds numbers, two main mechanisms, the adverse leading-edge pressure gradient and the shock-induced separation, can be expected to prevail. It is imperative that any dynamic stall flow control schemes that are developed be robust and effective against all dynamic stall onset mechanisms over the full range of flow conditions observed in the rotor flight envelope.

Specific to dynamic stall control is that the unsteady vorticity flux increases dramatically when an airfoil is rapidly pitched past the static stall angle. This is particularly interesting because one effect of unsteadiness is to reduce the equivalent angle of attack for the airfoil, which is responsible for the delay of stall measured. Eventually, this unsteady vorticity abruptly coalesces into the dynamic stall vortex. Generally, the vortex can form and grow in less than a half of a degree increase in angle of attack. Its subsequent convection over the airfoil induces undesirable pitching moment variations, which needs to be prevented for any control method to be deemed successful. Research by the authors[2] has shown that the dynamic stall vortex forms when the levels of vorticity flux exceed a critical threshold, a process that also depends strongly on the Mach number. In this context, it is helpful to analyze the following relation[5]:

$$\nu\frac{\partial\Omega}{\partial n} = \frac{\partial U_S}{\partial t} + \frac{1}{\rho}\frac{\partial p}{\partial s} + V\Omega \tag{1}$$

which states that the vorticity flux (left-hand side) is related to the airfoil surface acceleration (the unsteady term), the pressure gradient, and the surface transpiration (the last term). An examination of this equation in the light of the findings discussed in Ref. 3 suggests that dynamic stall control strategies should address ways to manipulate the flow vorticity field. Vorticity manipulation involves some means of shedding it gradually through the boundary layer and, thus,

Presented as Paper 99-3122 at the AIAA 17th Applied Aerodynamic Conference, Norfolk, VA, 28 June–1 July 1999; received 6 November 1999; revision received 27 June 2000; accepted for publication 8 September 2000.

*Research Professor and Associate Director, Department of Aeronautics and Astronautics; current mailing address, NASA Ames Research Center, M.S. 260-1, Moffett Field, CA 94035-1000. Associate Fellow AIAA.
†Senior Research Scientist, 690 W. Fremont Ave. Suite 8. Member AIAA.
‡Emeritus Scientist, U.S. Army Aviation and Missile Command and Experimental Physics Branch. Member AIAA.

not allowing it to coalesce. It appears that shedding the unsteady vorticity from some downstream location in smaller chunks of fluid can provide an acceptable solution to prevent the vortex from forming. Then the drastic consequences of the vortex-induced pitching moment variations can be avoided, even if the flow separates partially. As the equation indicates, using either surface acceleration[3] or surface mass transfer such as blowing and/or suction[6] enables some degree of vorticity flux manipulation. The latter has been a popular approach to control of steady flows, but has only been partly satisfactory in dynamic stall control for incompressible conditions. At higher freestream speeds, the rates of suction and injection needed are so large that the method becomes impractical.

The technique of oscillatory blowing[7–9] in which a nearly zero net mass flux is used with alternate blowing and suction at high amplitudes and frequencies has been shown to control incompressible dynamic stall. In tests[8,9] it was found that the blowing coefficient (defined as the ratio of oscillatory jet momentum, based on the blowing slot height and velocity to the freestream momentum) was in the range of 0.3–2%. These low values have made it an attractive and practical approach. The values depend on the maximum angle of attack relative to the static stall angle and the frequency of oscillation. It can be expected that much higher values will be needed with increasingly higher amplitude above the static stall angle because the flow separation will be stronger. Typical blowing frequencies can exceed several hundred hertz even at low Mach numbers. Thus far, the success of the method has been limited to control of dynamic stall of airfoils where trailing-edge flow separation is predominant. Its extension to higher freestream Mach numbers and to compressible dynamic stall, which occurs at the leading edge, has yet to be made.

Discussions in Ref. 9 indicate that it may also be necessary to employ oscillatory blowing at downstream locations on the airfoil rather than near the leading edge alone. It is clear that considerable work is still needed for a better evaluation of the applicability of this technique for controlling rotor flows.

Acoustic excitation[10] has also been used to control unsteady separated flows, but the acoustic power requirements increase disproportionately with increasing Mach number, and, thus, it does not appear to be practical for compressible dynamic stall control.

Two other methods of incompressible dynamic stall have been attempted with varying degrees of success. One used a slatted airfoil (Carr and McAlister[11]) wherein a leading-edge slat was employed to reduce the effective angle of attack of the airfoil. Tests in a water tunnel showed that an angle of attack as high as 34 deg could be reached without encountering either static or dynamic stall. The presence of a slat in the flow at low angles of attack, of course, introduces an increased drag penalty. This is especially critical on the high-speed advancing side of a rotor. Hence, a variation of this concept, the varying droop leading-edge (VDLE) airfoil, was explored by Yu et al.[12] In this, a segmented VR-12 airfoil was studied in a water tunnel. The droop of the leading 25% of the airfoil was mechanically changed to decrease its angle of attack on the advancing side and serve as a leading-edge slat on the retreating side. It was found that the design delayed static stall considerably. More importantly, unlike the basic VR-12 airfoil, which experienced strong leading-edge stall and developed a dynamic stall vortex, the drooped VR-12 airfoil did not suffer from either of these events even at $\alpha = 23$ deg. Only mild trailing-edge stall was observed. As a consequence, the force and moment loops were considerably smaller for the VDLE airfoil design. The performance of this airfoil at higher speeds remains to be established.

Geissler and Sobieczky[13] studied dynamic stall control through use of a variable camber airfoil. This computational study was aimed at demonstrating stall control by drooping the nose of an NACA 23012 airfoil to create a dynamically varying camber, with use of a special code to generate the variation of geometry in time. Effective control of dynamic stall was demonstrated at $M = 0.1$ up to $\alpha = 24.5$ deg. The dynamic stall vortex was eliminated for this incompressible case. However, a large region of trailing-edge separated flow was present. In comparison, a large dynamic stall vortex formed in the flow over a rigid airfoil. It produced the usual large excursions in the pitching moment. As the Mach number was increased, it was found that the effectiveness of the approach decreased. Although the onset of dynamic stall was delayed at $M = 0.3$ by drooping the airfoil nose, a smaller dynamic stall vortex was still produced, which remained on the surface even at $\alpha = 24.5$ deg. The peak negative pitching moment was significantly smaller. A supersonic bubble formed at this higher Mach number for both cases that was found to be responsible for some of the observed effects. The authors state that "complete suppression of the dynamic stall vortex is a much more difficult task."[13]

Based on the slatted airfoil studies of Ref. 11, a new two-element slatted airfoil[14] design was arrived at that was found to perform well in model rotor tests. This design has now been tested[14] for its compressible dynamic stall characteristics with two slat configurations.

It has been shown in Ref. 3 that compressible dynamic stall is very sensitive to airfoil leading-edge curvature. Because it is always a leading-edge type of stall, changing airfoil nose curvature can be an effective method of both steady and unsteady stall control. This is because of the effect of geometry change on the local adverse pressure gradient. This has been demonstrated in Ref. 3 by using a dynamically deforming leading-edge (DDLE) airfoil to control compressible dynamic stall. Real-time geometry modification was successfully employed to introduce major effects on the outer potential flow. The resulting dynamic changes in the overall pressure distribution on the airfoil produced the desired effect, thus providing the ability to manipulate the vorticity field. The control effectiveness was found to depend on several factors, such as rate of change curvature, angle of attack of initiation and termination of the geometry change, etc. This approach enabled shaping the airfoil nose as needed for each instantaneous flow condition, changing it from a sharp-nosed airfoil suitable for the advancing side flight to a round-nosed airfoil for the retreating side flight.

Before proceeding further, note that the slatted airfoil exhibits dynamic stall free behavior and attached flow up to $\alpha = 20$ deg when oscillated for incompressible freestream Mach numbers ($M < 0.2$) (Ref. 15). This becomes possible because the flow between the slat and the main airfoil produces a strong jet, which energizes the main element boundary layer. The unsteady vorticity of the slat is shed steadily through the main element airfoil during the pitch-up process. The DDLE airfoil was also found to be dynamic stall free at $M = 0.3$ for certain carefully selected shape change schedules.[3] The leading-edge flow was always attached with some trailing-edge separation, which served to shed the unsteady vorticity gradually.

This paper addresses the use of the DDLE airfoil and the slatted airfoil techniques for flow control at $M = 0.4$, a condition where the retreating blade of a rotor blade needs to perform without experiencing dynamic stall. The formation of shocks over the airfoil changes the dynamic of stall formation and the effectiveness of each method is altered significantly. Some of these effects are discussed here.

II. Description of the Experiment

The experiments were conducted in the NASA Ames Research Center, Fluid Mechanics Laboratory Compressible Dynamic Stall Facility (CDSF) using real-time point diffraction interferometry (PDI).

A. DDLE Airfoil

The description of the DDLE airfoil can be found in Ref. 3. It has a 6-in. chord, and in the undeformed state (shape-0) is an NACA 0012 airfoil, whose leading-edge profile can be changed to a semicircle with a diameter equal to the airfoil thickness at the 20% chord location. This is accomplished by pulling its nose in the chordwise direction by an amount less than 2 mm using a mandrel housed inside the airfoil. This 1.4% change in chord length translates to a 320% change in leading-edge radius of curvature. As can be expected, such a large change in the airfoil geometry yields a correspondingly significant change in the airfoil potential flow. The airfoil geometry change was first used to demonstrate[4] control of compressible, steady, separated flow at high angles of attack (α up to 18 deg). Subsequently, compressible dynamic stall over an oscillating airfoil was controlled[3] by dynamically changing its leading edge in a predetermined envelope. Some shapes generated using the

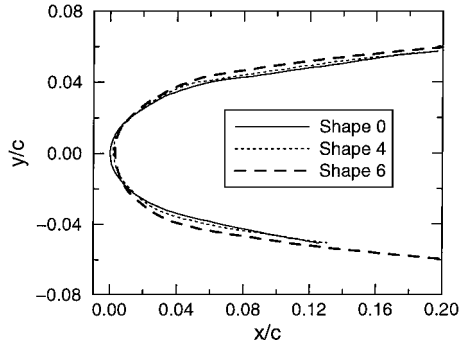

Fig. 1 DDLE airfoil shape profiles.

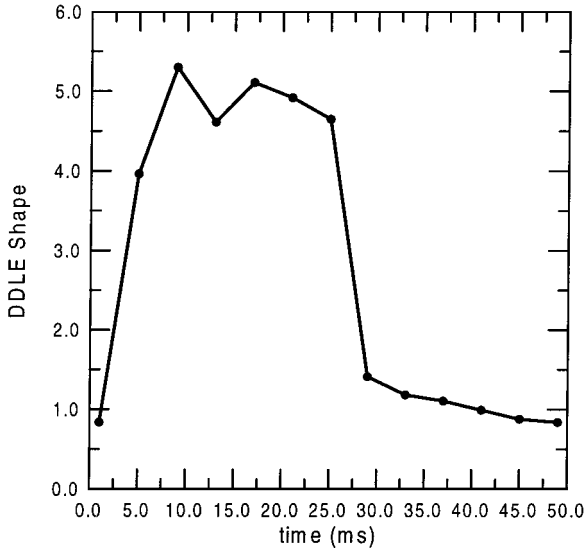

Fig. 2 Typical DDLE shape-change profile, $M = 0.4$ and $k = 0.05$.

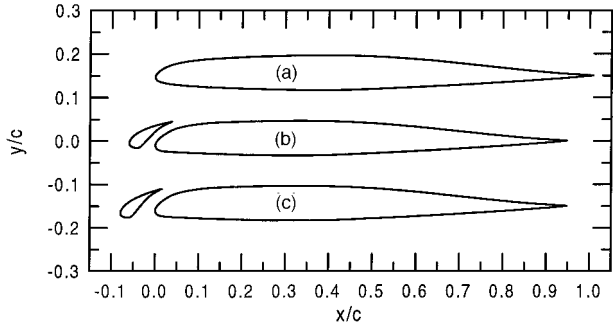

Fig. 3 Slatted airfoil profiles: a) RC(6)-08; b) RC(6)-08/106, 6-deg slat; and c) RC(6)-08/210, 10-deg slat.

present DDLE design are shown in Fig. 1. Here, each integer shape number represents a 0.003-in. chordwise movement of the leading edge from the preceding shape toward the trailing edge. Figure 2 shows a typical shape change profile used.

B. Slatted Airfoil

The slatted airfoil is a derivative of the basic 3-in. chord, 8% thick RC(6)-08 airfoil whose development details are given in Ref. 14. This is an airfoil designed specifically for the tip region of a rotor blade. Two slat configurations, a 6-deg slat, RC(6)-08/106 and a 10-deg slat, RC(6)-08/210, were tested. These geometries are shown in Fig. 3. The smaller chord of these airfoils permitted mounting them in the glass windows of the CDSF test section, allowing complete access to the airfoil flowfield.

C. Experimental Conditions

This paper presents results for the following experimental conditions: $M = 0.4$, $k = 0.05$, $\alpha = 10$ deg $+ 10$ deg $\sin\omega t$, $Re = 1.44 \times 10^6$ (DDLE airfoil) and 0.72×10^6 (RC airfoil), and range of shapes from shape-0 to shape-6. The range of DDLE shapes to be used for each Mach number was determined from an earlier study Ref. 3.

D. Experimental Uncertainties

The estimated uncertainties in the data are as follows: for Mach number, ± 0.005; for angle of attack, 0.05 deg; for reduced frequency, 0.005; for airfoil shape number, 0.05; for airfoil displacement, 4 μm; for C_p, ± 0.1; for $C_{p_{\min}}$, -5%; for $dCp/d(x/c)$, ± 25; and the change in α during DDLE movement is ± 0.25 deg.

III. Results and Discussions

In the following, the 6-in. chord DDLE airfoil results are compared with the 3-in. chord RC(6)-08 series airfoil. Shocks form at the test Mach number, and, hence, the density values corresponding to PDI fringe numbers cannot be converted to pressure values using isentropic relations (as was done for the lower Mach numbers[1–3]). In view of this and the Reynolds number difference between the two cases, only qualitative comparisons will be drawn. However, quantitative comparisons will be made within the sets wherever appropriate.

A. Flow over the Slatted Airfoil

Figure 4 shows the flow over the basic RC(6)-08, the 6-deg slat RC(6)-08/106 and the 10-deg slat RC(6)-08/210 airfoils at $M = 0.4$ and $k = 0.05$. It is very clear from the top row of Fig. 4 that dynamic stall occurs over the basic airfoil with a large vortex convecting over the upper surface. In fact, by $\alpha = 14.5$ deg, the airfoil is in deep dynamic stall. The 6-deg slat (middle row) seems to have successfully prevented the vortex from forming, although the slat itself experiences dynamic stall at high angles. The fringes over the middle of the airfoil upper surface resemble those of a vortex; however, a closer look reveals that these actually emanate from the leading edge of the stalled slat and do not enclose a vortex.[14] Beyond $\alpha = 16.5$ deg, full leading-edge separation results. In contrast, the bottom row (Fig. 4) for the 10-deg slat system show that at $\alpha = 16.4$ deg the flow remains attached on the main element due to slot blowing. In addition, the separated flow from the trailing edge of the slat attaches over the main element. However, stall develops shortly thereafter, and deep stall occurs by $\alpha = 18$ deg. Although the fringe pattern observed is akin to that seen during deep dynamic stall, it is clear that no dynamic stall vortex is present. This result implies that the pitching moment variations are likely to be milder compared to that obtained for the basic airfoil case. Note that full leading-edge stall occurred for all three cases, with the $\Delta\alpha$ over which it prevailed decreasing considerably with increase in the slat angle. Hence, it can be said that the slatted airfoil delivers a more desirable performance. Amongst the two slatted airfoil cases considered, the 10-deg slat is somewhat better in delaying deep stall onset.

B. Flow over the NACA 0012 and DDLE Airfoils

Figures 5 and 6 show the flow development over the NACA 0012 and the DDLE airfoils, respectively, at $M = 0.4$ and $k = 0.05$. Shocks develop over the former by $\alpha = 10$ deg (Fig. 5a) and shock-induced dynamic stall ensues by $\alpha = 10.5$ deg, (Fig. 5b) with deep dynamic stall following at $\alpha = 12.5$ deg as can be seen in Fig. 5c. Figures 5 show that the whole process occurs over a very small angle-of-attack range. The flow remains fully stalled until $\alpha \approx 10$ deg on the downstroke.

In contrast, the DDLE airfoil, whose shape is varied from shape 0 to shape 6 shows many different flow features. At $\alpha = 9$ deg, the flow over the leading edge is fully attached. A small separation bubble is seen beyond $x/c \approx 0.08$. The airfoil has been nearly deformed to shape 6 (which corresponds to a leading-edge movement of only 0.018 in.) by this angle. As the airfoil pitches up, shocks develop near the leading-edge region, and by $\alpha = 13$ deg (Fig. 6b, shape 5.7)

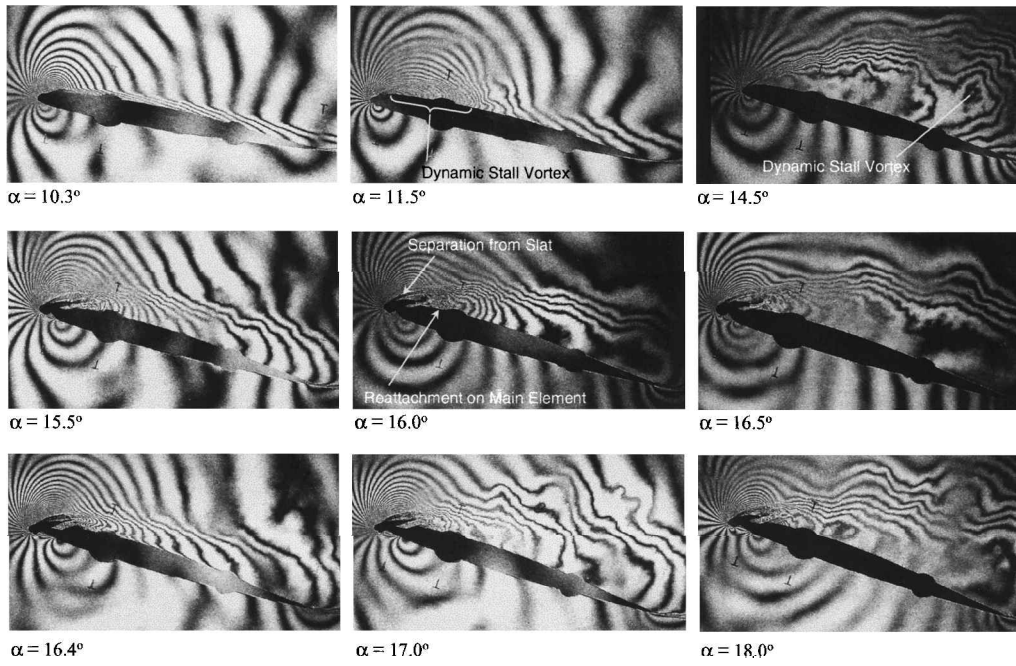

Fig. 4 PDI images of flow over the RC(6)-08 Airfoil, $M = 0.4$ and $k = 0.05$: top row, basic RC(6)-08 airfoil; middle row, RC(6)-08/106 airfoil; and bottom row, RC(6)-08/210 airfoil.

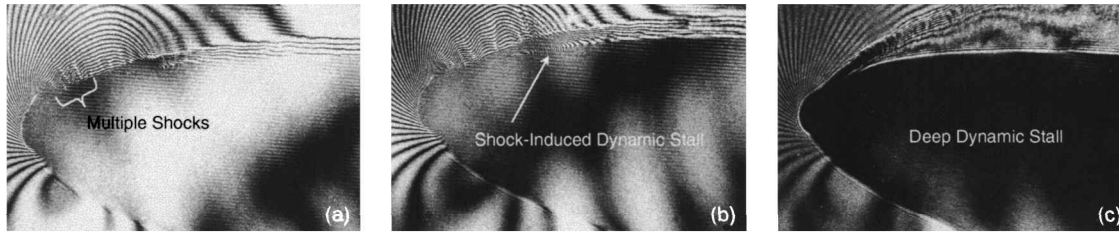

Fig. 5 PDI images of flow over the NACA 0012 airfoil, $M = 0.4$ and $k = 0.05$: a) $\alpha = 10.0$ deg, b) $\alpha = 10.5$ deg, and c) $\alpha = 12.5$ deg.

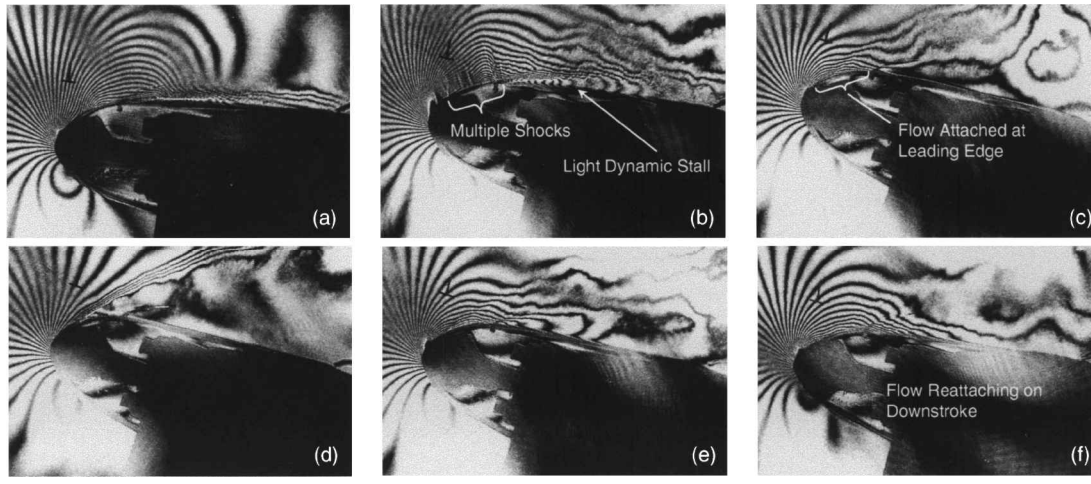

Fig. 6 PDI images of flow over the DDLE airfoil, $M = 0.4$ and $k = 0.05$: a) $\alpha = 9.0$ deg, shape 5.9; b) $\alpha = 13.0$ deg, shape 5.7; c) $\alpha = 19.0$ deg, shape 5.6; d) $\alpha = 20.0$ deg, shape 5.6; e) $\alpha = 18.1$ deg↓, shape 4.7; and f) $\alpha = 15.1$ deg↓, shape 1.5.

it appears that light dynamic stall is initiated on the upstroke, downstream from the foot of the shock. During this stage, the vorticity downstream of the shock is shed. This process continues as the airfoil pitches up and eventually stops by $\alpha = 19$ deg (Fig. 6c, shape 5.6). The leading-edge flow is fully attached, but with fewer fringes, implying a decreased peak suction value. The technique has been successful in delaying unsteady stall by about 7 deg when compared to the fixed NACA 0012 airfoil. Further increase in α results in a brief period of separation from the leading edge as shown in Fig. 6d for $\alpha = 20$ deg, shape 5.6. However, the leading-edge flow quickly reattaches (Fig. 6e, $\alpha = 18$ deg, shape 4.7) on the downstroke. By $\alpha = 16$ deg on the downstroke and shape 1.5 (Fig. 6f) while reforming the NACA 0012 airfoil, the flow has nearly fully reattached. Thus, the attached flow regime for the DDLE airfoil extends over a much larger angle-of-attack range than for the NACA 0012 airfoil. Most importantly, there is no organized dynamic stall vortex as was

seen for the NACA 0012 airfoil, and the airfoil produces suction lift for most of the oscillation cycle when the leading-edge flow remains attached. This behavior is almost similar to that seen for the fixed shape-6 airfoil (Ref. 3) whose leading edge flow was attached throughout the cycle. Because the airfoil has to change its shape for acceptable performance on the advancing side, a slight leading-edge separation without the dynamic stall vortex may be a modest price to pay. Furthermore, the decreased drag possibility of this design on the advancing side makes it preferred method for controlling the rotor dynamic stall flow.

C. Comparison of Airfoil Peak Suction Pressure Coefficient

The peak suction pressure coefficient, $C_{p_{\min}}$ determined from a counting of the fringes for the various airfoils is shown in Fig. 7. A comparison of the values for the basic RC(6)-08 airfoil and the 10-deg slat airfoil shows that the slatted airfoil can develop peak suction to a higher angles of attack ($\alpha = 16.5$ deg) compared to the basic airfoil ($\alpha = 11$ deg). Furthermore, the peak value is slightly higher at about -4.2 compared to -3.5 for the basic shape. This indicates that the slat is effective not only in controlling dynamic stall, as was seen earlier, but also in enabling suction lift generation in the process. It is well known that as the airfoil stalls either statically or dynamically, the values fall. The more gradual fall for the slatted airfoil case indicates that its stall behavior has been changed to the trailing-edge type, which proceeds much more gradually, unlike the abrupt onset and progression seen for the NACA 0012 airfoil and the basic RC(6)-08 airfoil flows, which also show the presence of a large dynamic stall vortex. This is because, even when the slat stalls, the bleed flow through the slot keeps the main element boundary layer energized, which introduces a significant change in the flow vorticity dynamics. The small amount of unsteady vorticity (because of the small slat size and lower effective angle of attack) built up due to pitching is shed from the slat. The low level of vorticity locally appears to be the reason why it does not coalesce. Instead, it merges with the boundary-layer vorticity on the main element. As a result, the rapid movement of the center of pressure responsible for the large pitching moment variations is absent, and, hence, a better pitching moment distribution results.

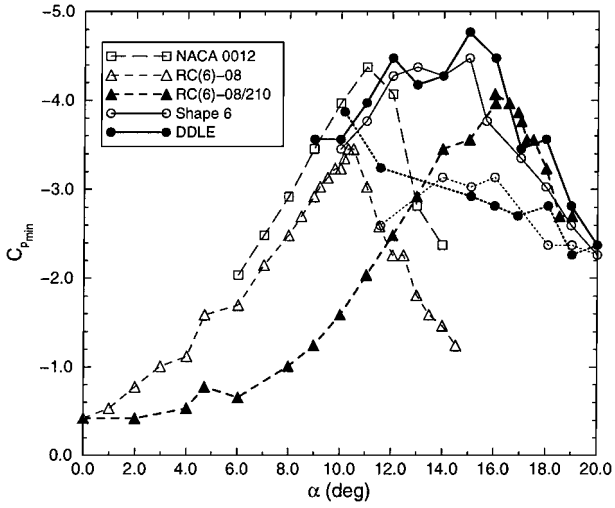

Fig. 7 Development of suction peak on various airfoil configurations for $M = 0.4$ and $k = 0.05$.

In comparison, the shape adaptive airfoil flow develops an even higher peak suction pressure of -4.9, a value attained at $\alpha = 16$ deg. Also note that the $C_{p_{\min}}$ plot appears like the natural extension of the NACA 0012 airfoil as its shape is adapted. The loss of the suction peak occurs at a rate comparable to that observed for the slatted airfoil, but as the flow visualization pictures discussed earlier revealed, the recovery is also quicker, and by $\alpha = 16$ deg on the downstroke the value is fairly high at ≈ -3.4. Despite the small amount of flow separation seen, it can be concluded from Fig. 7 that acceptable shape adaptation can be achieved for this flow condition.

Figure 7 also shows the $C_{p_{\min}}$ distribution for the shape-6 airfoil, which was found to be dynamic stall vortex free in Ref. 3. Note the similarity of its peak suction variation with angle of attack and that of the shape adaptive airfoil through the dynamic stall angles-of-attack range. The shape adaptive airfoil, however, generally develops about 15–20% higher peak suction values, which is clearly desirable. Thus, shape adaptation, which is necessary to satisfy the geometry requirements on the advancing side, is also beneficial. The reason for the increased suction peak pressures appears to be the favorable interaction between the two unsteady timescales present in the flow, namely, the airfoil reduced frequency and the shape adaptation rate, both of which contribute to the unsteady term in the vorticity flux equation. Together, these seem to induce a pronounced effect on

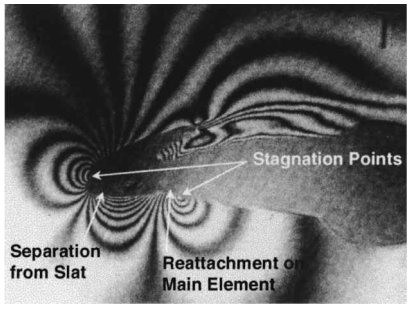

a) $\alpha = 4.0$ deg

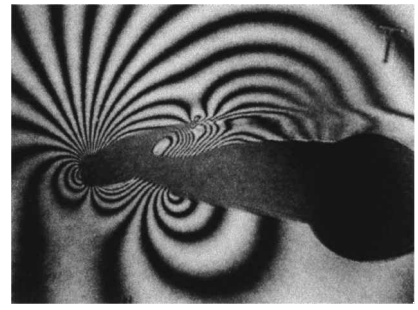

b) $\alpha = 9.0$ deg

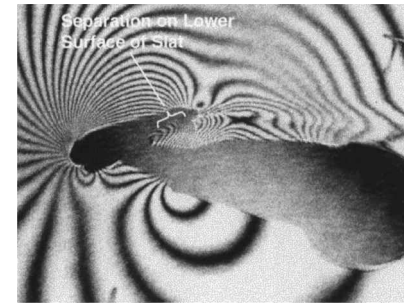

c) $\alpha = 14.0$ deg

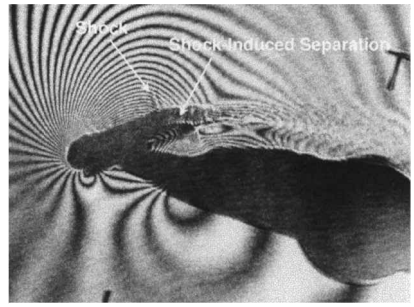

d) $\alpha = 15.6$ deg

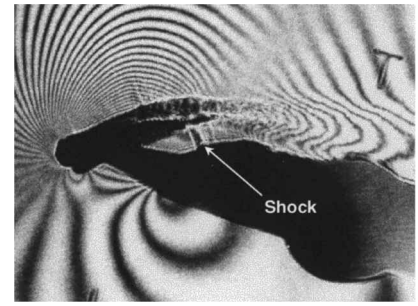

e) $\alpha = 16.4$ deg

Fig. 8 PDI images of flow over the leading-edge slat of the RC(6)-08/210 airfoil, $M = 0.4$ and $k = 0.05$.

the vorticity flux manipulation. This interaction is not present in the slatted airfoil flow, but the bleed flow through the slot [the third term on the right-hand side of Eq. (1)] produces an equivalent effect, but to a lesser extent judging by the range of $\Delta\alpha$ over which the flow was separated for the slatted airfoil case.

D. Effect of Flow Through the Slot

At higher Mach numbers, the performance that can be derived from a slatted airfoil case reaches a limit due to the details described hereafter. In the following, only the case of the RC(6)-08/210 design is discussed because it exhibited a more desirable performance in delaying dynamic stall. The flow through the slot separates at low angles of attack and becomes restricted due to choking at higher angles. Figure 8 presents representative interferograms for this case. Figure 8a shows that, at $\alpha = 4$ deg, the flow separates from the leading edge of the slat and actually reattaches on the lower surface of the main element. Thus, there is little flow through the slot. However, at this angle, the main element flow is attached. Even the shear layer emanating from the trailing-edge of the slat reattaches to the airfoil upper surface. Hence, the separation from the slat lower surface is not of much consequence. At $\alpha = 9$ deg, the slot flow has increased as can be inferred from the fringes that have turned into the passage. It appears that the slat trailing-edge shear layer reattaches farther downstream on the main element. There is a small separation region near the trailing edge on the slat pressure side, which forces the slot jet flow to stay closer to the main element leading edge (Fig. 8c, $\alpha = 14$ deg). With further pitchup of the airfoil, a shock forms on the upper surface of the slat (Fig. 8d, $\alpha = 15.6$ deg). The shock forms irrespective of the slot blowing effect on the main airfoil and induces separation on the slat. The abrupt thickening of the boundary layer seen in Fig. 8d is clear evidence of this. By $\alpha = 16.4$ deg, a shock forms in the slot passage also, and it nearly occupies the full height of the slot (Fig. 8e). The slot can become choked, and, thus, the maximum improvement of stall control reaches its limit. Further gains can only be obtained if the passage area is increased, which can lead to structural problems, in addition to further increase in drag on the advancing side.

Another interesting aspect of the choked slot flow is that, for this condition, in the specific case of the RC(6)-08/210, an effective blowing coefficient of about 15–20% was realized, which is a significantly large number and may explain the success observed with this design.

The preceding results indicate that practical implementation of a slatted airfoil design for rotor flow control is much more challenging because the freestream Mach number varies from low subsonic to supersonic depending on the rotor azimuth angle.

IV. Conclusions

A comparative study of two widely different approaches for compressible dynamic stall control has been carried out. One involved the use of a slatted airfoil, and the other used the DDLE airfoil approach. The dynamic stall flow over these two geometries was studied at conditions of interest to a rotor blade, in particular, at $M = 0.4$, $k = 0.05$, and $\alpha = 10 \text{ deg} + 10 \text{ deg} \sin\omega t$. Both methods proved successful in suppressing the destructive dynamic stall vortex by modifying the vorticity field differently.

The DDLE airfoil test results reported depend on the airfoil shape adaptation schedule used. It is possible to optimize the schedule to minimize the separated flow regime, which is of considerable interest to rotorcraft design. Measurable improvement in the blade performance can be obtained, even if only the leading-edge flow remains attached. One of the major advantages of the DDLE approach is its ability to shape the airfoil for both the advancing and retreating side flight conditions of the rotor blade. Determination of the appropriate deformation schedule is a very involved task.

The slatted airfoil is mechanically simple and is quite effective in suppressing the dynamic stall vortex. However, flow separation from the slat lower surface at low angles of attack, the drag due to this, the presence of the slat on the advancing side, the conflicting requirements of optimizing the slat configuration over the full range of rotor conditions, and the limit placed by the choking slot flow are significant issues.

The state of the art is such that it may not be possible to attain a flow control situation where separation is completely prevented. However, for a rotor, the goal is to avoid the formation of the dynamic stall vortex. This has been achieved for airfoil dynamic stall conditions. From the results and reasoning presented here, it appears that the DDLE airfoil concept holds a slight edge over other means of flow control attempted. It is hoped that the rapid developments occurring in the field of smart materials and microactuators will enable designing the actuators to produce the small range of leading-edge movement needed to achieve the stated goal on full scale rotors.

Acknowledgments

The DDLE work was supported by a research Grant (MIPR8BNPSARO07) from the U.S. Army Research Office. The slatted airfoil research was supported by the U.S. Army Aeroflightdynamics Directorate. The support of S. S. Davis, Fluid Mechanics Laboratory of NASA Ames Research Center and the assistance of R. A. Miller in model installation and the control system are gratefully acknowledged.

References

[1]Carr, L. W., "Progress in Analysis and Prediction of Dynamic Stall," *Journal of Aircraft*, Vol. 25, No. 1, 1988, pp. 6–17.

[2]Chandrasekhara, M. S., Wilder, M. C., and Carr, L. W., "Competing Mechanisms of Compressible Dynamic Stall," *AIAA Journal*, Vol. 36, No. 4, 1998, pp. 387–393.

[3]Chandrasekhara, M. S., Wilder, M. C., and Carr, L. W., "Compressible Dynamic Stall Control Using a Shape Adaptive Airfoil," AIAA Paper 99-0650, Jan. 1999.

[4]Chandrasekhara, M. S., Wilder, M. C., and Carr, L. W., "Unsteady Stall Control Using Dynamically Deforming Airfoils," *AIAA Journal*, Vol. 36, No. 10, 1998, pp. 1792–1799.

[5]Reynolds, W. C., and Carr, L. W., "Review of Unsteady, Driven, Separated Flows," AIAA Paper 85-0527, March 1985.

[6]Alrefai, M., and Acharya, M., "Controlled Leading-Edge Suction for the Management of Unsteady Separation over Pitching Airfoils," AIAA Paper 95-2188, June 1995.

[7]Seifert, A., Bahcar, T., Koss, D., Shepshelovich, M., and Wygnanski, I., "Oscillatory Blowing: A Tool to Delay Boundary Layer Separation," *AIAA Journal*, Vol. 31, No. 11, 1993, pp. 2052–2060.

[8]Greenblatt, D., Darabi, A., Nishri, B., and Wygnanski, I., "Separation Control by Periodic Addition of Momentum with Particular Emphasis on Dynamic Stall," American Helicopter Society Paper T3-4, April 1998.

[9]Greenblatt, D., and Wygnanski, I., "Dynamic Stall Control by Oscillatory Forcing," AIAA Paper 98-0676, Jan. 1998.

[10]Ahuja, K. K., and Burrin, R. H., "Control of Flow Separation," AIAA Paper 84-2298, Oct. 1984.

[11]Carr, L. W., and McAlister, K. W., "The Effect of a Leading-Edge Slat on Dynamic Stall of an Oscillating Airfoil," AIAA Paper 83-2533, Oct. 1983.

[12]Yu, Y. H., Lee, S., McAlister, K. W., Tung, C., and Wang, C. M., "Dynamic Stall Control for Advanced Rotorcraft Applications," *AIAA Journal*, Vol. 33, No. 2, 1995, pp. 289–295.

[13]Geissler, W., and Sobieczky, H., "Dynamic Stall Control by Variable Airfoil Camber," CP-522, AGARD, 1995, pp. 6.1–6.10.

[14]Noonan, K. W., "Aerodynamic Characteristics of a Rotorcraft Airfoil Designed for the Tip Region of a Main Rotor Blade," NASA TM 4264, 1991.

[15]Carr, L. W., Chandrasekhara, M. S., Wilder, M. C., and Noonan, K. W., "The Effect of Compressibility on Suppression of Dynamic Stall Using a Slotted Airfoil," AIAA Paper 98-0332, Jan. 1998.